


Article

Duncan–Chang E - ν Model Considering the Thixotropy of Clay in the Zhanjiang Formation

Bin Tang ^{1,*}, Tianli Liu ²  and Biaohe Zhou ³

¹ Guangxi Key Laboratory of Geotechnical Mechanics and Engineering, Guilin University of Technology, Guilin 541004, China

² School of Civil and Architectural Engineering, Guilin University of Technology, Guilin 541004, China

³ College of Civil Engineering, Tongji University, Shanghai 200092, China

* Correspondence: tangbin@glut.edu.cn

Abstract: The clays of the Zhanjiang Formation in the coastal area of Beibu Gulf of China are thixotropic, and the existing constitutive relationship models relevant for clay are incapable of accurately simulating their stress–strain relationships. It is vital to study the changes of mechanical properties of Zhanjiang Formation clay that occur during thixotropy, and to establish a constitutive model considering thixotropy. The varying measures of its shear strength, cohesion, internal friction angle, and initial tangential modulus during thixotropy were investigated by means of triaxial consolidation and drainage tests. Furthermore, the quantitative relationships between the clay’s cohesion, internal friction angle, and initial tangential modulus of the clay and time were examined. This relationship was introduced into the Duncan–Chang model, and a Duncan–Chang model considering the thixotropy of clay was developed. The established model was used to make predictions to assume the validation of the experimental data, and numerical simulations were then carried out. All of the results from the model’s prediction, numerical simulation and experimental measurements were compared against each other in order to verify the reasonableness of the model we had utilized. The results positively demonstrated that: (1) the shear strength, cohesion, angle of internal friction, and initial tangent modulus of the clay gradually increases with longer curing times, and eventually it will stabilize; and (2) compared with the Duncan–Chang model not considering thixotropy, the established thixotropic model is better able to reflect the influence of clay thixotropy on the clay stress–strain relationship, as its mean relative error is smaller. The results of this study provide references for calculating strength and deformation of the clay thixotropy. Further, it also provides references for bearing load calculations of pile foundations in thixotropic clay strata when subjected to long-term loading conditions.



Citation: Tang, B.; Liu, T.; Zhou, B. Duncan–Chang E - ν Model Considering the Thixotropy of Clay in the Zhanjiang Formation. *Sustainability* **2022**, *14*, 12258. <https://doi.org/10.3390/su141912258>

Academic Editors: Chao Jia, Kai Yao and Shuai Shao

Received: 26 July 2022

Accepted: 23 September 2022

Published: 27 September 2022

Publisher’s Note: MDPI stays neutral with regard to jurisdictional claims in published maps and institutional affiliations.



Copyright: © 2022 by the authors. Licensee MDPI, Basel, Switzerland. This article is an open access article distributed under the terms and conditions of the Creative Commons Attribution (CC BY) license (<https://creativecommons.org/licenses/by/4.0/>).

Keywords: Zhanjiang Formation clay; thixotropy of clay; initial tangential modulus; Duncan–Chang model; thixotropic model

1. Introduction

Sustainable economic development cannot be achieved without the aid of infrastructure construction. In recent years, a large number of infrastructure construction projects, such as Baosteel Zhanjiang Iron & Steel and Zhongke Refinery and Petrochemical Complex Integration Project, have been initiated in the coastal area of Beibu Gulf. Zhanjiang Formation clay is widely distributed in these regions, the infrastructure projects mostly use Zhanjiang Formation clay as foundation. Due to its strong structural and thixotropic properties, this gifts it rare engineering properties, making it an extremely unusual and special soil. The special nature of Zhanjiang Formation clay contributes to the complexity of bearing properties of infrastructure foundation and groundwork. Therefore, it is important to study the special properties of Zhanjiang Formation clay in order to assess the sustainable development of the coastal economy.

The Zhanjiang Formation, located in the coastal area of Beibu Gulf, China, is a river-controlled delta-phase sedimentary layer primarily composed of three types of clastic materials (sand, gravel, and clay), with incomplete deposition patterns of coarse material in lower layers and fine in the upper. Among them, the clay of the Zhanjiang Group is widely exposed on the surface or subducted under the Quaternary Holocene soil or Middle Pleistocene soil, which is the main carrier of various engineering activities. The clays found in this region have high plasticity, spatial distribution variability, strong structural properties, and thixotropy. Together, this leads to an extremely unusual and special soil which possesses rare mechanical properties.

The thixotropy of clay refers to the gradual variations of its mechanical properties resulting from a period of resting time after a clay structure has been destroyed [1–4]. The presence of thixotropy causes the stress–strain relationship of the clay to vary with resting time, as its strength and deformation properties are both highly time-dependent [5–8].

The effect of thixotropy on the strength and deformation properties of clays was initially investigated by Tang [9] through an unconfined compressive strength test, which showed that the strength of the tested clays increased gradually as resting periods carried on, with an eventual stabilization. During the thixotropic process, the strength of the clay is rapidly augmented in the early stage, slows down in the middle stage, and gradually evens out in the later stage. Zhang [10] further examined the strength–growth law, as well as the thixotropic mechanism of clay throughout this process by simultaneously conducting macroscopic and microscopic tests. The results of the testing showed that after a period of 500 days, the strength of clay had been multiplied to 2.58 times what it had been at the outset. Zhang also found that the internal structure of clay during thixotropy underwent adaptive adjustment, and that the degree of cementation between the particles had also gradually increased. Later, Shahriar [11] studied the effect of thixotropy on the one-dimensional compressive properties of clay, pointing out that settlement calculations obtained using the traditional effective stress principle had to be strictly modified to accommodate for effective vertical stresses reading as less than 100 kPa. Alam [12] closely examined both the strength and deformation properties of clay during thixotropy. The findings revealed that the yield stress of clay increased with the passing of time, which proved that there was a proportional relationship between the thixotropic strength ratio and the plasticity index. Seng [13] studied the effects of thixotropy on the shear modulus of clays with different water content. Results showed that the higher the water content of the clay, the more significant the effect of thixotropy on the shear modulus. These studies indicate that the presence of thixotropy leads to the strength and deformation modulus of clay being closely related to time, and also that the influence of clay thixotropy should be considered when performing geotechnical calculations.

The models most commonly used to reflect the stress–strain relationship of soil are the linear elastic model, the Duncan–Chang model, the Mohr–Coulomb model, the D–P model, and the modified Cambridge model. Among these, the linear elastic model factors in just two elastic parameters of the soil, reflecting the linear relationship of stress–strain. The Duncan–Chang model approximates the plastic deformation of the soil by making adjustments to the elastic parameters, reflecting the non-linear and simple characteristics of the stress–strain curve of the soil. The Mohr–Coulomb model evaluates two elastic parameters and three plastic parameters of the soil, which works to more accurately describe the damage behavior of the soil. The D–P model makes appropriate modifications to the yield surface function of the Mohr–Coulomb model to make it easier to carry out numerical calculations. The modified Cambridge model takes into account two elastic parameters, three plastic parameters, two state parameters and one parameter which controls the shape of the soil’s yield surface, which results in a more defined description of the elastic-plastic deformation characteristics of the soil, while concurrently taking into account the plastic volume deformation of the soil. One drawback to these conventional models. However, the existing constitutive model lacks the capacity to integrate the effect of clay thixotropy when simulating stress–strain relationships, resulting in inaccurate simulations. The study of the

impact that thixotropy bears on the stress–strain relationship of clays, and the development of a model for accurately calculating the stress–strain relationship which takes thixotropy into account, are of great significance in extending and improving the constitutive theory of clays.

In relation to the different computational models commonly used when considering thixotropy, Dexter [14] studied the thixotropy of German and Israeli soils by means of penetration tests. He was then able to describe the thixotropic behavior of soils by focusing on particle rearrangement, which led to his development of two simplified mechanical models of clay thixotropy based on the results of these tests. Barnes [15] provided two additional approaches to modeling thixotropy based on viscous and viscoelastic theories, respectively. Dullaert [16] further proposed a general structural dynamics model in order to describe the flow behavior of thixotropic systems in inelastic suspension media. This was accomplished by evaluating a series of system transient experiments caused by sudden changes in shear rate and by considering structural damage and structural recovery. Chao [17] proposed modelling strain rate versus time for clay, based on triaxial compression test data of soft clay. Tang [18] proposed a model for strength recovery during the process of thixotropy of clay, after studying the effects of moisture content, density, and sensitivity. All of these studies have provided contributive ideas for considering the thixotropy of clay in geotechnical calculations. However, due to the absence of describing the quantitative relationship between the stress–strain relationship and time for clay during the thixotropy process, these models struggle to accurately describe the stress–strain relations for clay in the general stress state during thixotropy. As a result, their application in geotechnical calculations is limited, and further research is still needed.

In this paper, the clay of Zhanjiang Formation was selected as the main focus of our study of the variation of stress–strain relationship during the thixotropy process of clay. We also aim to extend the intrinsic relationship model applied to thixotropic clay. The stress–strain relationship of clay when under different curing times is studied in this paper by means of triaxial consolidation and drainage tests. The shear strength and initial tangential modulus of the specimens at different curing times were obtained according to the stress–strain relationship of the specimens at different curing times. Further, the cohesive force and internal friction angle of the specimen at different curing times were determined according to the shear strength of the gathered specimens. The quantitative relationship between time and the cohesion, internal friction angle, initial tangential modulus of the specimen is established. This quantitative relationship is introduced into the Duncan–Chang model to establish a constitutive model considering the thixotropy of clay. The UMAT subroutine of this specific model was developed in Fortran language and embedded in the ABAQUS program in order to simulate the test. This model was used to predict the test data validation under different curing times. The model's prediction results, numerical simulation results, and experiment results were subsequently compared to verify the efficiency of the model.

2. Materials and Methods

2.1. Experimental Study of the Thixotropy of Clay

The tested specimen was taken from the Baosteel project site in Donghai Island, Zhanjiang City, Guangdong Province. It was documented with a natural moisture content of 40.17%, a natural density of 1.80 g/cm³, and a specific gravity of solid particles of 2.71. The soil sample collected was dried naturally, crushed, and then filtered through a 2 mm sieve, with any soil samples with a particle size of less than 2 mm being added to distilled water to configure its moisture content to the natural moisture content. The specimen was then transformed into a cylindrical specimen with a diameter of 39.1 mm and a height of 80 mm, wrapped in cling film, and placed into a pre-prepared constant temperature and humidity curing box. The temperature was set at 25 °C. The resting time was determined to be 7 days. The strength of the clay gradually increases with the increase in resting time, and eventually stabilizes [9]. Therefore, the amount of resting time between each group of tests was designed to gradually increase. One resting time was interleaved for tests 1, 2 and 3;

two resting times for tests 3, 4 and 5; three resting times for tests 5, 6 and 7; and four resting times for tests 7 and 8. Thus, the curing time calculated for each group of tests was 1 day, 7 days, 14 days, 28 days, 42 days, 63 days, 84 days, and 112 days, respectively (1 day was used as the initial curing age for the purpose of establishing the logarithmic relationship between cohesion, angle of internal friction, and initial tangential modulus versus time). Triaxial consolidation and drainage tests were carried out on all specimens at end of each age of curing (with 100 kPa, 200 kPa, and 300 kPa confining pressures, respectively), and stress–strain relationship curves were obtained for specimens at different curing times and confining pressures, as shown below in Figure 1.

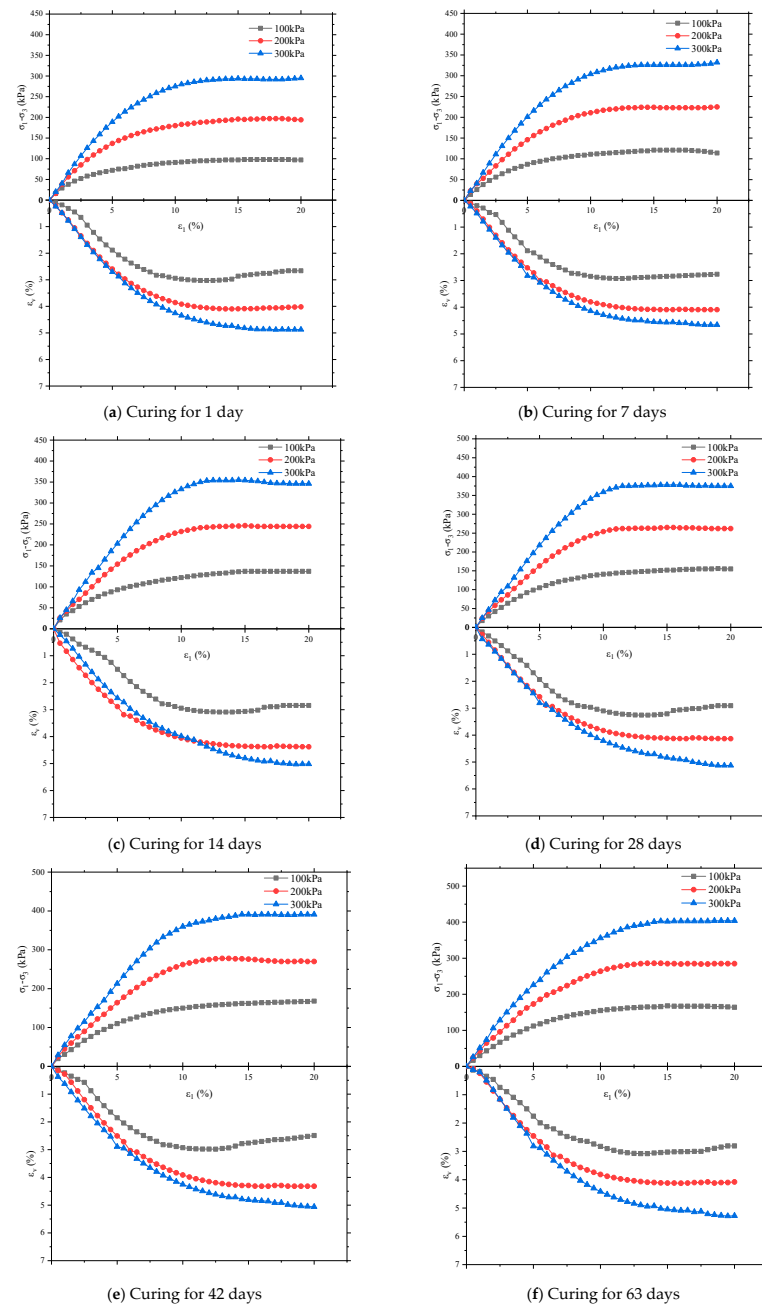


Figure 1. Cont.

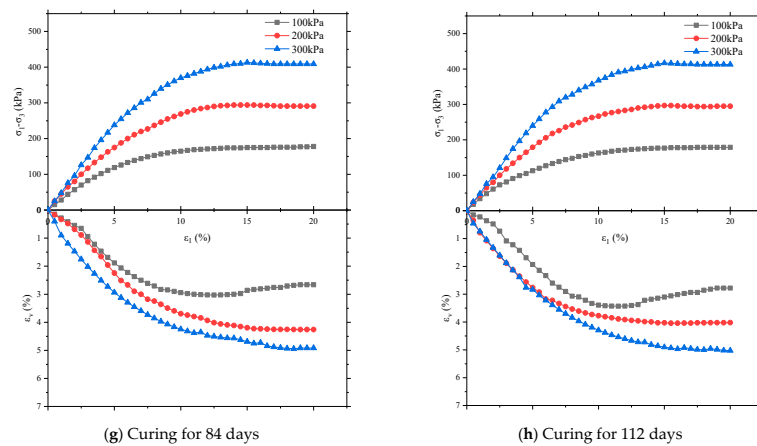


Figure 1. Stress–strain relationship curve for specimens with different curing times.

2.1.1. Effect of Thixotropy on the Shear Strength of Clay

From Figure 1, it can clearly be seen that the stress on the clay being observed gradually increases with the increase in strain under the same curing time and confining pressure. The figure also highlights that the stress of the specimen tends to stabilize once the strain of the specimen reaches 15%. Under the same curing time, when the specimen finally stabilizes, the stress gradually increases with the increase in the confining pressure. Furthermore, under the same confining pressure, when the specimen finally reaches stability, the stress gradually increases with the increase in curing time. Therefore, the stress, which corresponds to 15% of the strain, was taken as the shear strength of the specimen, and then the shear strength of the specimen was plotted against the curing time, as shown in Figure 2.

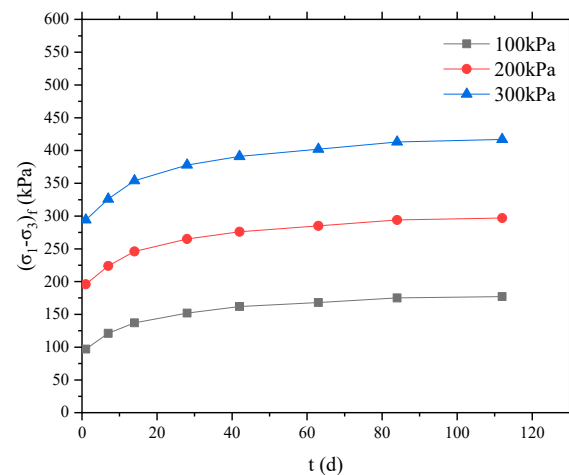


Figure 2. The relationship between the strength of the specimen and the curing time.

Looking at Figure 2, it is evident that the strength of the specimens gradually increased concurrently with increase in the curing time, eventually reaching a state of stabilization. This is due to the clay re-forming a new stable structure with the increase in time [19–22]. Huo [23] studied the thixotropy of soft clay in Tianjin and analyzed the internal mechanism of clay thixotropic behavior. The results of the study showed that, during the thixotropy process, the soil particles follow the principle of energy minimum to re-flocculate and re-agglomerate, leading to the formation of a new stable structure. Additionally, the strength of the soil then gradually increased. Zhang [24] analyzed the recovery process of Zhanjiang clay in terms of its thixotropic strength, studying the clay's structural changes when it underwent thixotropic transition. It was concluded that the development of its structure from dispersion to flocculation under the action of gravitational and repulsive

forces between clay particles was the main reason for the recovery of strength during clay thixotropy. Shen [25] analyzed how the mechanical properties of high-sensitivity marine clay varied by conducting indoor tests. Results from these experiments showed the long time change of clay properties was due to consolidation and cementation during thixotropic recovery. Tang [26] studied the unconfined compressive strength and pore structure evolution law in the thixotropic process through unconfined compressive strength test, scanning electron microscopy, and mercury injection test. The results showed that, in the process of thixotropy, the soil particles gradually coagulate and form an aggregates flocculation structure, and the strength of clay increases with the increase in the degree of cementation.

Based on the strength at each curing time and the confining pressure of the test, several things were achieved: the Mohr circle of each age specimen was plotted, the cohesion and internal friction angle of each age specimen were determined, the cohesion and internal friction angle of the specimens were plotted versus the curing time, and a logarithmic fit was performed. The results from all of this are shown in Figure 3.

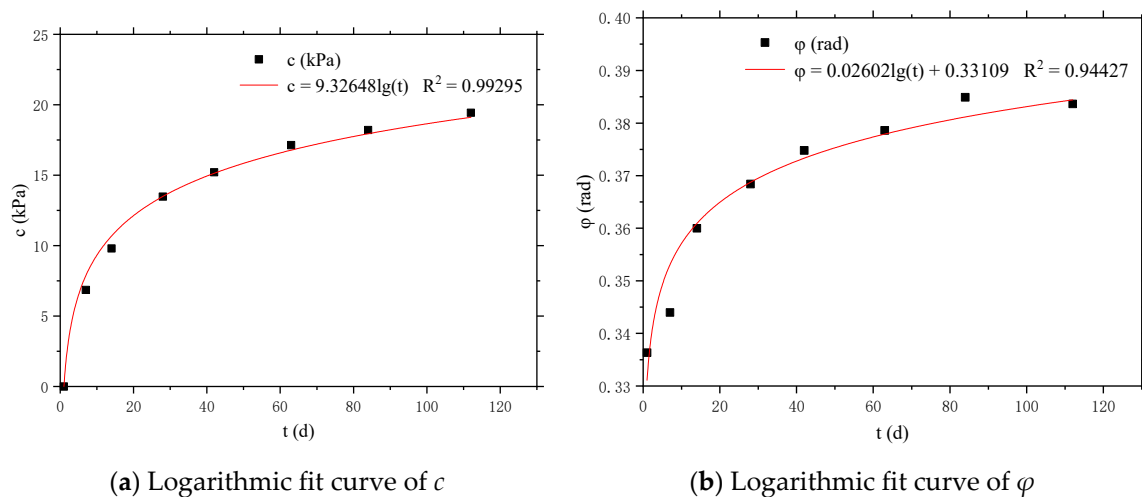


Figure 3. Curves of c and φ versus curing time.

Figure 3 demonstrates that the cohesion and the angle of internal friction of the clay gradually increased along with the increase in the curing time, after which it finally levels off. The cohesion and internal friction angle are both related to the curing time, shown as follows:

$$c = A \text{ (kPa) } \lg(t/d) \quad (1)$$

$$\varphi = B \lg(t/d) + \varphi_0 \quad (2)$$

In this equation, c is the cohesive force of the specimen (kPa), and A is the parameter of the influence of thixotropy on the cohesive force, with a scale of 1. It was found that the larger the value of A , the greater the influence of thixotropy on the cohesive force, and vice versa. Further, t is the curing time (d); φ is the angle of internal friction of the specimen (rad), and B is the parameter of the influence of thixotropy on the angle of internal friction, with a scale of 1. It was found that the larger the value of B , the greater the effect of thixotropy on the angle of internal friction, and vice versa. Finally, φ_0 is the angle of internal friction at the initial moment of the specimen (rad).

In order to ensure the consistency of the scale on both sides of Equations (1) and (2), multiply A by 1 kPa and divide t by 1 d.

2.1.2. Effect of Thixotropy on the Deformation Properties of Clay

To further investigate the effect of thixotropy on the deformation properties of clay, the initial tangential modulus of each age specimen was taken in order to establish its unique relationship with the curing time. From Figure 1, it can be seen that the stress–strain

relationship curve of the specimens is a hardened curve, which can be described by the Duncan–Chang model [27]. When using this model, the initial tangential modulus of the specimen can be found by the following equation:

$$\varepsilon_1/(\sigma_1 - \sigma_3) = a + b \varepsilon_1 \quad (3)$$

$$E_i = 1/a \quad (4)$$

Here, ε_1 is the axial strain of the specimen with a scale of 1, $(\sigma_1 - \sigma_3)$ is the deviatoric stress (kPa), a and b are the regression parameters, respectively, and E_i is the initial tangential modulus of the specimen (kPa).

The data in Figure 1 were regressed using Equation (3) in order to determine the parameter a . The initial tangential modulus of each specimen was determined by substituting it into Equation (4), plotting the initial tangential modulus of the specimen against the curing time, and then performing a logarithmic fit, with the results shown in Figure 4.

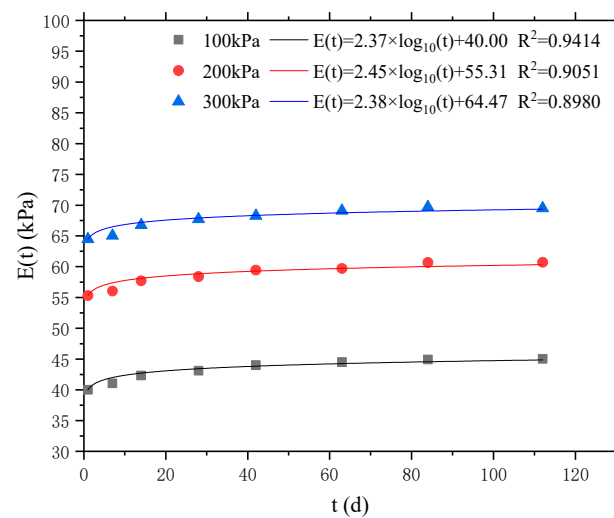


Figure 4. Logarithmic fitting curve of the initial tangential modulus with curing time.

From Figure 4, it can be seen that the initial tangential modulus of the specimens gradually increases in direct correlation to the extension of the conservation time, eventually stabilizing later on. The initial tangential modulus of the specimen is related to the curing time as follows:

$$E_i(t) = C \text{ (kPa)} \lg(t/d) + E_i \quad (5)$$

Detailing the equation above, $E_i(t)$ is the initial tangential modulus of the specimen at conservation time t (kPa), and C is the parameter of the influence of thixotropy on the initial tangential modulus of the clay, with a scale of 1. The greater the value of C , the greater the influence of thixotropy on the initial modulus, and vice versa; also, t is the conservation time (d), and E_i is the initial tangential modulus of the specimen at the initial moment (kPa).

To ensure the consistency of the magnitudes on both sides of Equation (5), multiply C by 1 kPa and divide t by 1 d.

As shown by Figure 4, the influence of the confining pressure on the magnitude of C value is not significant; thus, the C value can be taken as its average value. The influence of the confining pressure on the initial tangential modulus E_i of the specimen at the initial moment is also evident due to the compressive stiffness of the clay, and it can be calculated by the following equation of compressive stiffness [27]:

$$E_i = K_E Pa (\sigma_3/Pa)^n \quad (6)$$

where: E_i is the compression modulus (kPa); K_E and n are constants with a scale of 1, and Pa is the atmospheric pressure (kPa).

It can be seen from Equation (6) that the compression modulus E_i is a power function of the confining pressure σ_3 . As such, when both K_E and n are greater than 0, the compression modulus E_i increases with the increase in the confining pressure σ_3 . Using Equation (6) to fit a power function to the initial tangential modulus E_i of the initial moment pattern garners such results as shown in Figure 5.

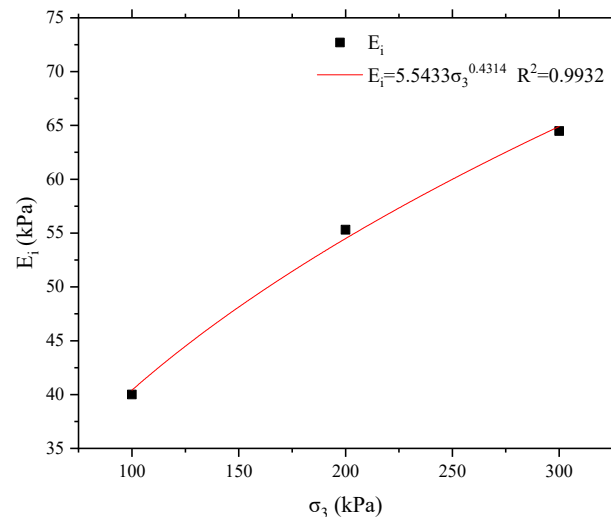


Figure 5. Power function fitting curve of E_i versus confining pressure.

As can be seen from Figure 5, Equation (6) reflects the relationship between E_i and the confining pressure efficiently. Substituting Equation (6) into Equation (5) yields the initial tangential modulus of the specimen versus the confining pressure, shown as:

$$E_i(t) = C \text{ (kPa)} \lg(t/d) + K_E Pa (\sigma_3/Pa)^n \quad (7)$$

2.2. Duncan–Chang Model Considering Thixotropy

According to the results of the triaxial consolidation and drainage tests mentioned above, the stress–strain relationship of the specimens during thixotropy in the clay of the Zhanjiang Formation bears obvious non-linear characteristics, with the Duncan–Chang model [27] being better able to simulate the non-linear stress–strain relationship of clay. Even still, the Duncan–Chang model cannot consider the influence of the thixotropy of clay. One suggestion for improving this model would be introducing a thixotropy parameter to allow for the influence of the thixotropy of clay.

The Duncan–Chang model is a type of E - v model in which the basic parameters of the soil sample can be obtained from both conventional triaxial consolidation as well as drainage tests. The tangential modulus E_t is thus determined from the relationship curve between the deviatoric stress ($\sigma_1 - \sigma_3$) and the axial strain ε_1 , and the tangential Poisson's ratio ν_t is subsequently determined from the relationship curve between the axial strain, ε_1 , and the horizontal strain, ε_3 .

2.2.1. Deviatoric Stress–Axial Strain Relationship Considering Thixotropy

In the Duncan–Chang model, the relationship between the deviatoric stress ($\sigma_1 - \sigma_3$) and the axial strain, ε_1 , in the soil is assumed to be hyperbolic [27], i.e.,:

$$\sigma_1 - \sigma_3 = \varepsilon_1 / (a + b \varepsilon_1) \quad (8)$$

Above, a and b are the hyperbolic parameters, respectively.

According to the definition of the modulus of elasticity, in the incremental method, the tangential modulus can be defined as:

$$E_t = d\sigma_1 / d\varepsilon_1 \quad (9)$$

Since this is the case, substituting Equation (8) into Equation (9) yields:

$$E_t = \frac{d\sigma_1}{d\varepsilon_1} = \frac{d(\sigma_1 - \sigma_3)}{d\varepsilon_1} = \frac{1}{a + b\varepsilon_1} - \frac{b\varepsilon_1}{(a + b\varepsilon_1)^2} \quad (10)$$

From Equation (10), the value of E_t tends to $1/a$ when ε_1 tends to 0, indicating that the parameter a is the inverse of the initial tangential modulus E_i of the $(\sigma_1 - \sigma_3)$ - ε_1 relationship curve, i.e.,:

$$a = 1/E_i \quad (11)$$

From Equation (8), the value of $(\sigma_1 - \sigma_3)$ tends to $1/b$ when ε_1 tends toward positive infinity, indicating that the parameter b is the inverse of the limiting value of $(\sigma_1 - \sigma_3)$, i.e.,:

$$b = 1/(\sigma_1 - \sigma_3)_{ult} \quad (12)$$

In practice, the axial strain ε_1 of the specimen cannot reach infinity, leading to the specimen being damaged when a large deformation of the specimen occurs. In conventional triaxial tests, the stress at 15% axial strain is generally taken to be the damage load $(\sigma_1 - \sigma_3)_f$ of the specimen, necessitating that a damage ratio R_f [27] needs to be introduced, which can be shown as:

$$R_f = (\sigma_1 - \sigma_3)_f / (\sigma_1 - \sigma_3)_{ult} \quad (13)$$

The damage ratio R_f is generally taken as an empirical value of 0.75 to 1 [27].

Substituting Equation (7) into Equation (11) yields the expression for the hyperbolic parameter a considering the effect of thixotropy as:

$$a = \frac{1}{E_i(t)} = \frac{1}{C \text{ (kPa)} \lg\left(\frac{t}{d}\right) + K_E Pa \left(\frac{\sigma_3}{Pa}\right)^n} \quad (14)$$

Substituting Equation (13) into Equation (12) gives the expression for the hyperbolic parameter b as:

$$b = 1/(\sigma_1 - \sigma_3)_{ult} = R_f / (\sigma_1 - \sigma_3)_f \quad (15)$$

According to the Mohr–Coulomb theory, it is known that the specimen breaks with:

$$(1/2) (\sigma_1 - \sigma_3) - (1/2) (\sigma_1 + \sigma_3) \sin\varphi - c \cos\varphi = 0 \quad (16)$$

From Equation (16) the expression for the strength of the specimen can be obtained as:

$$(\sigma_1 - \sigma_3)_f = (2c \cos\varphi + 2\sigma_3 \sin\varphi) / (1 - \sin\varphi) \quad (17)$$

Substituting Equation (17) into Equation (15) yields:

$$b = R_f (1 - \sin\varphi) / (2c \cos\varphi + 2\sigma_3 \sin\varphi) \quad (18)$$

Substituting Equation (1) and Equation (2) into Equation (18) gives the expression for the hyperbolic parameter b , taking into account thixotropy, as:

$$b = \frac{R_f \{1 - \sin[B \lg\left(\frac{t}{d}\right) + \varphi_0]\}}{2A \text{ (kPa)} \lg\left(\frac{t}{d}\right) \cos[B \lg\left(\frac{t}{d}\right) + \varphi_0] + 2\sigma_3 \sin[B \lg\left(\frac{t}{d}\right) + \varphi_0]} \quad (19)$$

Substituting Equations (14) and (19) into Equation (8) gives the relational expression for $(\sigma_1 - \sigma_3)$ - ε_1 , considering thixotropy, as:

$$\sigma_1 - \sigma_3 = \frac{\varepsilon_1}{\frac{1}{E_i(t)} + \frac{R_f (1 - \sin\varphi) \varepsilon_1}{2c \cos\varphi + 2\sigma_3 \sin\varphi}} \quad (20)$$

In this equation: $c = A \text{ (kPa)} \lg(t/d)$;

$\varphi = B \lg(t/d) + \varphi_0$;

$E_i(t) = C \text{ (kPa)} \lg(t/d) + K_E Pa (\sigma_3/Pa)^n$.

2.2.2. Determination of Tangential Modulus

For non-linear stress–strain relationships, the deformation of the soil, although non-linear, can be regarded as linear at small increment. Such deformation adheres to Hooke’s law. Both the tangential modulus and Poisson’s ratio are important elements of the non-linear elastic model. The method of determining the tangential modulus, E_t , is discussed below.

A transformation of Equation (8) yields:

$$\varepsilon_1 = (\sigma_1 - \sigma_3) a / [1 - (\sigma_1 - \sigma_3) b] \quad (21)$$

Substituting Equations (14) and (15) into Equation (21) yields:

$$\varepsilon_1 = \frac{\sigma_1 - \sigma_3}{E_i(t) \left[1 - \frac{R_f (\sigma_1 - \sigma_3)}{(\sigma_1 - \sigma_3)_f} \right]} \quad (22)$$

Differentiating the two sides of Equation (22) yields:

$$d\varepsilon_1 = \frac{d\sigma_1}{E_i(t) \left[1 - \frac{R_f (\sigma_1 - \sigma_3)}{(\sigma_1 - \sigma_3)_f} \right]^2} \quad (23)$$

Therefore, the tangential modulus can be expressed as:

$$E_t = \frac{d\sigma_1}{d\varepsilon_1} = E_i(t) \left[1 - \frac{R_f (\sigma_1 - \sigma_3)}{(\sigma_1 - \sigma_3)_f} \right]^2 \quad (24)$$

i.e.,:

$$E_t = E_i(t) \left[1 - \frac{R_f (\sigma_1 - \sigma_3) (1 - \sin \varphi)}{2c \cos \varphi + 2\sigma_3 \sin \varphi} \right]^2 \quad (25)$$

As shown, $c = A$ (kPa) $\lg(t/d)$;

$\varphi = B \lg(t/d) + \varphi_0$;

$E_i(t) = C$ (kPa) $\lg(t/d) + K_E Pa (\sigma_3/Pa)^n$.

2.2.3. Volume Strain–Axial Relationship Curves

The relationship curve for ε_1 – ε_3 is also assumed to be hyperbolic in the Duncan–Chang model [27], i.e.,:

$$\varepsilon_1 = -\varepsilon_3 / (f - D \varepsilon_3) \quad (26)$$

It can also be expressed as:

$$\varepsilon_3 = -f \varepsilon_1 / (1 - D \varepsilon_1) \quad (27)$$

When expressed as the latter, f and D are the hyperbolic parameters, respectively.

Moreover, when, for parameter D , the different curves can be averaged, then for parameter f , Duncan–Chang assumes the following relationship between parameter f and the confining pressure σ_3 :

$$f = G - F \lg(\sigma_3/\text{kPa}) \quad (28)$$

The values of the parameters G and F in Equation (28) can be derived by fitting the curve in accordance with different values of the confining pressure σ_3 and the corresponding f values.

The volumetric strain under conventional triaxial test conditions can then be expressed as:

$$\varepsilon_v = \varepsilon_1 + 2\varepsilon_3 \quad (29)$$

Substituting Equation (27) and Equation (28) into Equation (29) yields:

$$\varepsilon_v = \varepsilon_1 - \frac{2f \varepsilon_1}{1 - D \varepsilon_1} = \varepsilon_1 - \frac{2[G - F \lg(\frac{\sigma_3}{\text{kPa}})] \varepsilon_1}{1 - D \varepsilon_1} \quad (30)$$

From Equation (30), it can be seen that the parameters of the volumetric strain versus axial strain curves are D , G , and F . This trio of parameters can be obtained by either conventional triaxial consolidation or drainage tests.

2.2.4. Determination of Tangential Poisson's Ratio

The tangential Poisson's ratio is defined as:

$$v_t = -d\varepsilon_3/d\varepsilon_1 \quad (31)$$

Differentiating the two sides of Equation (27) yields:

$$d\varepsilon_3 = -f d\varepsilon_1/(1 - D \varepsilon_1)^2 \quad (32)$$

While substituting Equation (32) into Equation (31) yields:

$$v_t = -d\varepsilon_3/d\varepsilon_1 = f/(1 - D \varepsilon_1)^2 \quad (33)$$

Substituting Equation (22) and Equation (28) into Equation (33) yields:

$$v_t = -\frac{d\varepsilon_3}{d\varepsilon_1} = \frac{G - F \lg\left(\frac{\sigma_3}{\text{kPa}}\right)}{\left\{1 - \frac{D (\sigma_1 - \sigma_3)}{E_i(t) \left[1 - \frac{R_f (\sigma_1 - \sigma_3)}{(\sigma_1 - \sigma_3)_f}\right]}\right\}^2} \quad (34)$$

As shown above, $(\sigma_1 - \sigma_3)_f = (2c \cos \varphi + 2\sigma_3 \sin \varphi)/(1 - \sin \varphi)$

$c = A$ (kPa) $\lg(t/d)$;

$\varphi = B \lg(t/d) + \varphi_0$;

$E_i(t) = C$ (kPa) $\lg(t/d) + K_E Pa (\sigma_3/Pa)^n$.

3. Discussion and Validations of the Results

3.1. Discussion of the Results

In summary, the parameters of the improved Duncan–Chang model are R_f , φ_0 , A , B , C , K_E , n , D , G , and F . These ten parameters can be determined by using conventional triaxial consolidation and drainage tests. Parameter R_f is the damage ratio, i.e., the ratio of damage strength in relation to ultimate strength; φ_0 is the angle of internal friction of the specimen recorded at the initial moment of thixotropy; parameters A , B , and C are the parameters representing the influence of thixotropy on the cohesion of clay, the angle of internal friction, and the initial tangential modulus, respectively, as was discussed previously in Section 2; parameters K_E and n are both parameters reflecting the compressive stiffness of the soil (in these instances, the larger the value, the greater the initial tangential modulus with the increasing of the confining pressure, and the greater the stiffness of the soil, and vice versa); parameters D , G , and F are parameters factoring into the Duncan–Chang model that detail the hyperbolic relationship that exists between the strain in the horizontal direction of the specimen and the axial strain. The improved Duncan–Chang model introduces the different parameters of the influence of thixotropy on clay cohesion, angle of internal friction and initial tangent modulus. Thus, the improved Duncan–Chang model is applicable to clay with thixotropy. For sandy soils, $c = 0$ is preferred; also, for clay soils that do not exhibit significant thixotropy, $A = B = C = 0$ is preferred (in this case, the computational model becomes the Duncan–Chang model without the consideration of clay thixotropy). The following values of these model parameters were determined as a result of the test data gathered in Section 2, with the results shown below in Table 1.

Table 1. Table of model parameters.

φ_0	A	B	C	K_E	n	D	G	F	R_f
0.3311	9.466	0.02252	2.400	5.544	0.4314	0.01874	0.5921	0.1471	0.7500

3.2. Model Validations

3.2.1. Experimental Validations

In order to verify the efficiency of the improved Duncan–Chang model, we adjusted the curing time and the confining pressure for the tests in Section 2. The new curing times were set to 10 days, 50 days, and 90 days, with the confining pressure for the tests being set to 150 kPa, 250 kPa, and 350 kPa, respectively. We therefore used this established model to predict the outcome of the test results; according to the test conditions and the model parameters given in Table 1, we calculated the values of the hyperbolic parameters a and b for the relationship between the deviatoric stress ($\sigma_1 - \sigma_3$) and the axial strain ε_1 , which are highlighted in the following Tables 2 and 3.

Table 2. Predicted values of hyperbolic parameter a .

Curing Duration (Days)	150 kPa	250 kPa	350 kPa
10	0.01978	0.01602	0.01393
50	0.01915	0.01560	0.01361
90	0.01892	0.01545	0.01350

Table 3. Predicted values for hyperbolic parameter b .

Curing Duration (Days)	150 kPa	250 kPa	350 kPa
10	0.003954	0.002517	0.001846
50	0.003405	0.002234	0.001663
90	0.003236	0.002144	0.001603

The relationship prediction curve of $(\sigma_1 - \sigma_3)$ - ε_1 for the specimens was obtained by substituting Tables 2 and 3 into Equation (8); also, the relationship prediction curves of $\varepsilon_v - \varepsilon_1$ for the specimens was obtained by substituting the values of parameters D , G , F , as well as the confining pressure, into Equation (30); and finally, the prediction curves of the improved Duncan–Chang model were compared with the measured results of tests, as can be seen in Figure 6.

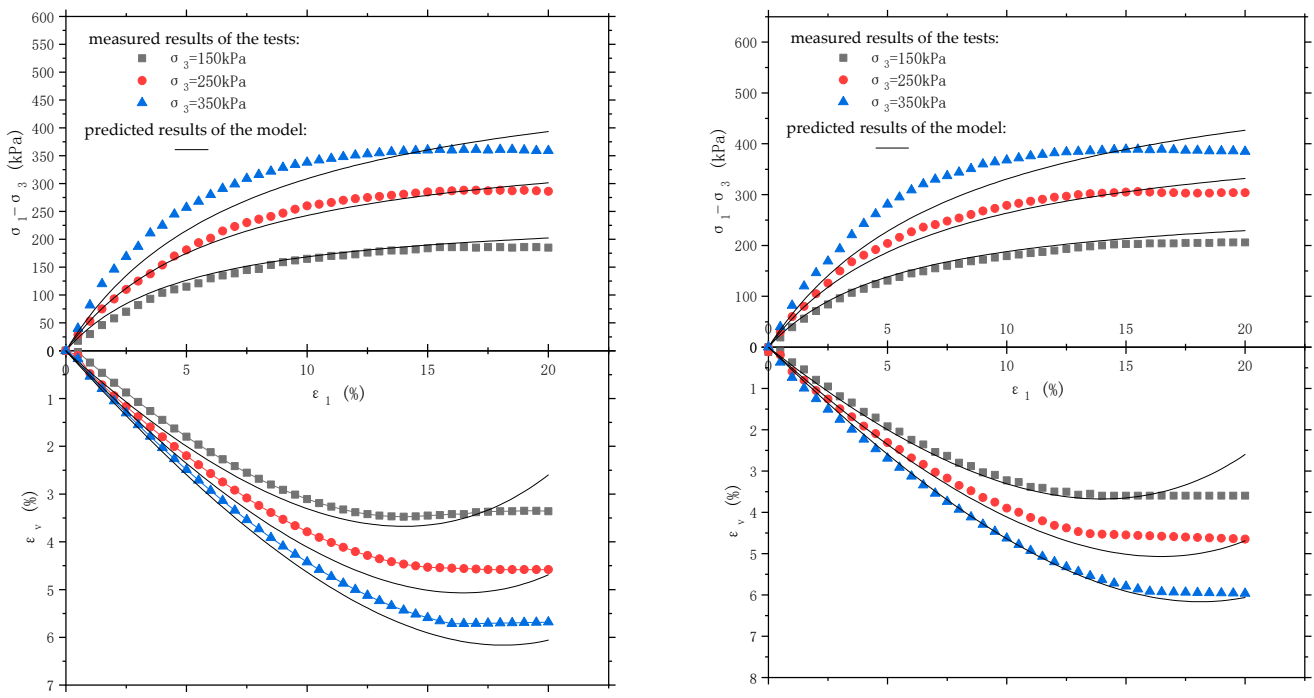
The mean relative errors observed between these model prediction results and the experimental measured results of $\sigma_1 - \sigma_3$ and ε_v in Figure 6 are highlighted in Tables 4 and 5.

Table 4. The mean relative errors between the model prediction results and the experimental measured results of $\sigma_1 - \sigma_3$.

Curing Duration (Days)	150 kPa	250 kPa	350 kPa
10	8.11%	3.44%	9.87%
50	6.89%	5.37%	10.61%
90	4.23%	4.72%	9.33%

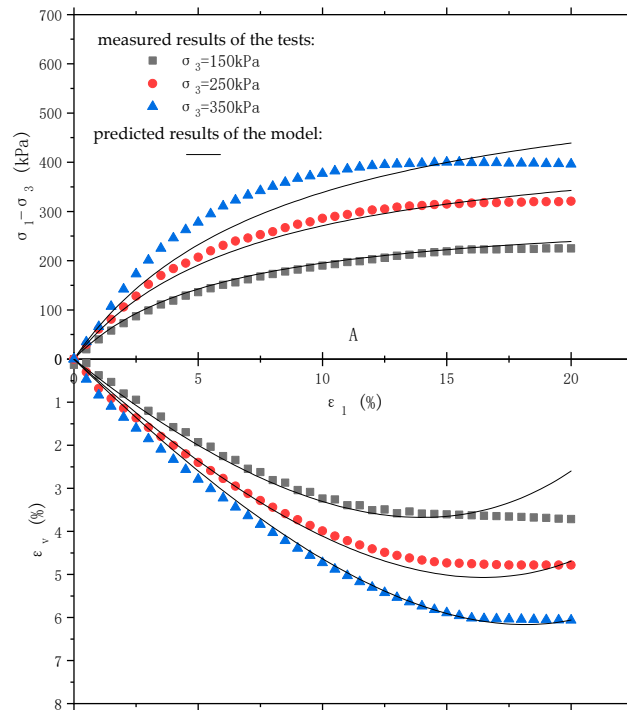
Table 5. The mean relative errors between the model prediction results and the experimental measured results of ε_v .

Curing Duration (Days)	150 kPa	250 kPa	350 kPa
10	30.53%	11.72%	6.60%
50	9.41%	6.47%	4.09%
90	10.27%	4.88%	5.75%



(a) Curing for 10 days

(b) Curing for 50 days



(c) Curing for 90 days

Figure 6. Comparison between the predicted results of the model and the measured results of tests.

Figure 6 and Tables 4 and 5 prove that the predicted results of the model were in good agreement with the measured results of tests, its mean relative error was small, indicating that the model developed was more accurate in reflecting how the thixotropy of the clay directly affected the non-linear stress–strain relationship of the clay.

Both prediction curves of the Duncan–Chang model—one not considering the thixotropy of the clay and one that did consider it—were compared against the measured results of

the tests for the curing time of 90 days and different confining pressures, with the results displayed in Figure 7.

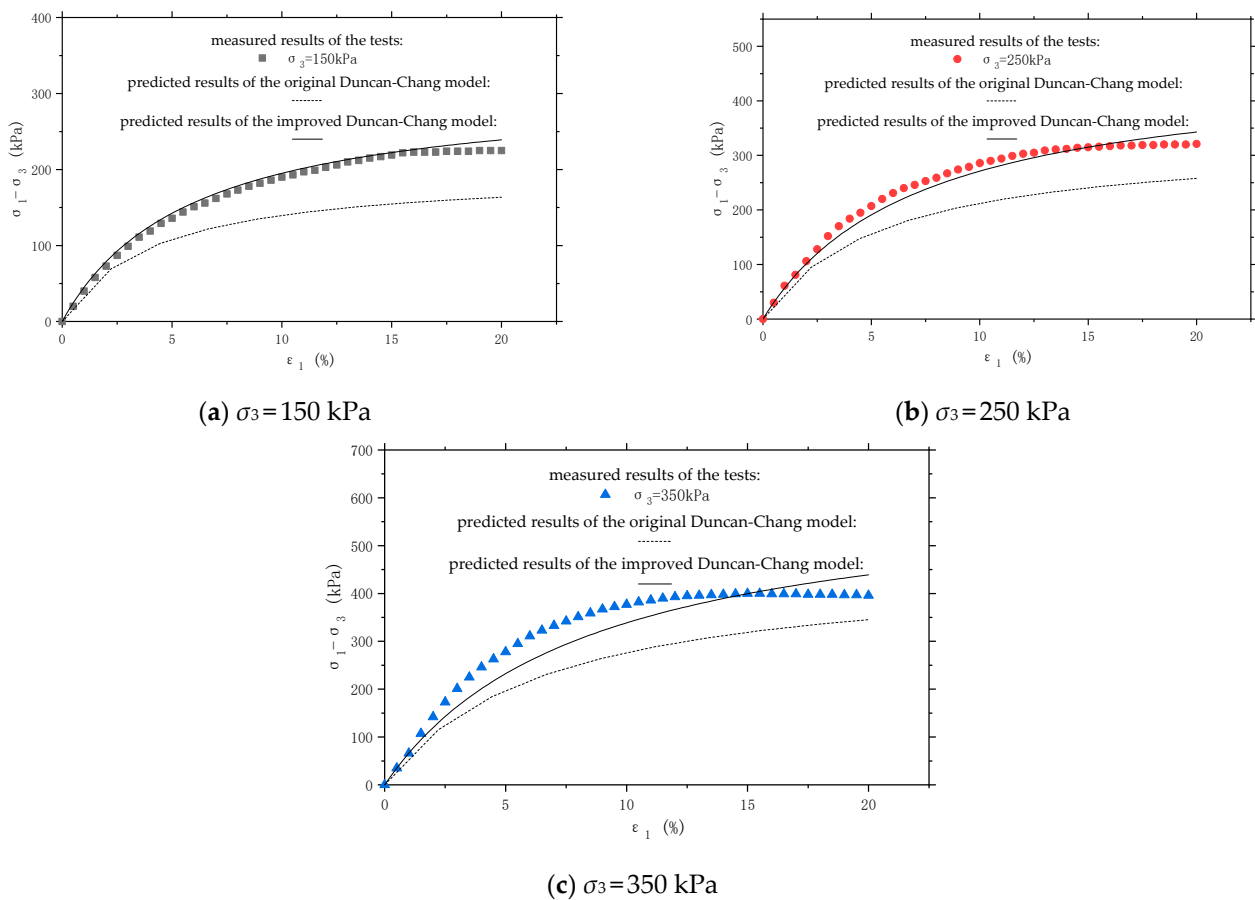


Figure 7. Comparison between the predicted results of the model and the measured results of tests.

The mean relative errors observed between these model prediction results and the experimental measured results of $\sigma_1 - \sigma_3$ in Figure 7 are highlighted in Table 6.

Table 6. The mean relative errors between the model prediction results and the experimental measured results of $\sigma_1 - \sigma_3$.

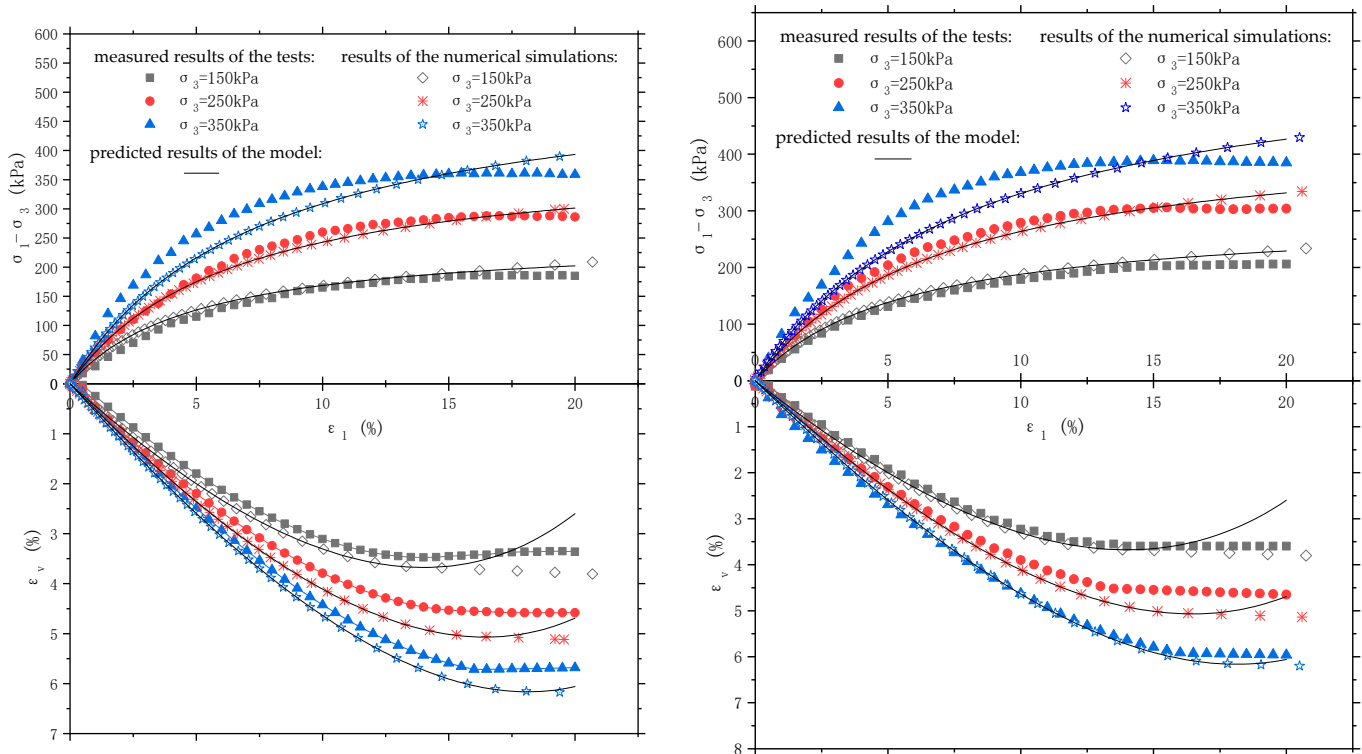
Duncan–Chang Model	150 kPa	250 kPa	350 kPa
Not considering Thixotropy	23.07%	22.24%	22.27%
Thixotropic	4.23%	4.72%	9.33%

Examining Figure 7 and Table 6, it can be seen that the Duncan–Chang model that considered the thixotropy of the clay reflected the stress–strain relationship of thixotropic clay more accurately than the model that did not consider thixotropy. Furthermore, its mean relative error was smaller, indicating that the established model is more suited to reflect the influence of thixotropy on the nonlinear stress–strain relationship of clay.

3.2.2. Numerical Simulation Validations

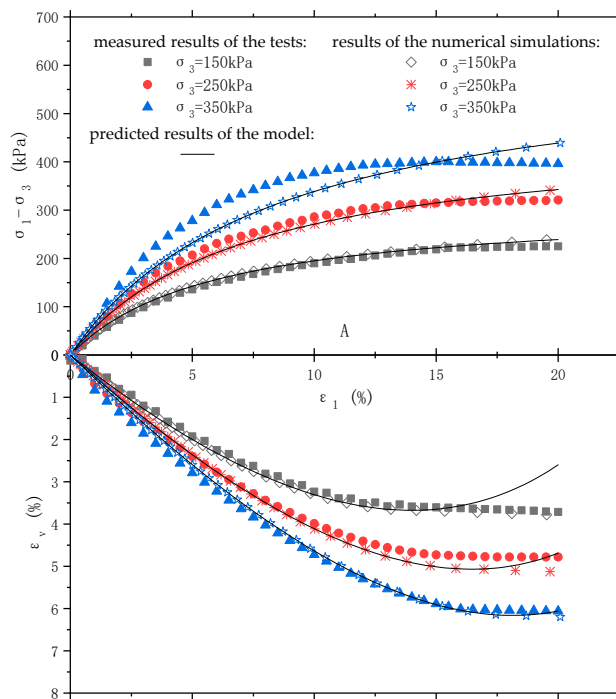
In order to further verify the validity of the proposed method, the ABAQUS software was used to simulate tests. The results of the numerical simulation, the predicted results of the model, and the measured results of tests were weighed against each other for validation. As there is currently no constructive model allowing for the thixotropy of clay in the ABAQUS software, the model was written as a UMAT subroutine in Fortran language and then subsequently embedded in the ABAQUS software. This enabled us to realize the

simulation of the thixotropy of clay. The results of the simulation of the test according to the above conditions are presented in Figure 8.



(a) Curing for 10 days

(b) Curing for 50 days



(c) Curing for 90 days

Figure 8. Comparison of the measured results of the experiment, the predicted results of the model, and the numerical simulation results.

As can be seen from Figure 8, the results of the numerical simulations, the measured results of tests and the predicted results of the model were in agreement, adding further validity to the developed model.

4. Conclusions

- (1) The shear strength, cohesion, and angle of internal friction of the clay gradually increases directly with the increase in the maintenance time, eventually stabilizing. Among these given factors, the relationship between cohesion, angle of internal friction, and maintenance time can all be expressed using a logarithmic function.
- (2) The initial tangent modulus of the clay gradually increases in harmony with the increase in the maintenance time before eventually reaching stabilization; the relationship between the initial tangent modulus and the maintenance time can also be expressed using a logarithmic function.
- (3) Compared with the Duncan–Chang model not considering thixotropy, the thixotropic model that was applied in this paper can more accurately reflect the influence of clay thixotropy on the clay stress–strain relationship, given its smaller mean relative error.

Author Contributions: Conceptualization, B.T.; writing—original draft preparation, B.Z.; writing—review and editing, T.L. All authors have read and agreed to the published version of the manuscript.

Funding: This research was funded by the National Natural Science Foundation of China, grant number 41867035; the Guangxi Natural Science Foundation, grant number 2020GXNSFAA297199; and the Project of Guangxi Key Laboratory of Geotechnical Mechanics and Engineering, grant number 2016-A-01.

Institutional Review Board Statement: Not applicable.

Informed Consent Statement: Not applicable.

Data Availability Statement: The data presented in this study are available on request from the corresponding author via e-mail: tangbin@glut.edu.cn.

Acknowledgments: We thank the funders, thank the helpful comments from the editors and reviewers, and thank the contributions of all authors.

Conflicts of Interest: The authors declare no conflict of interest.

References

1. Ren, Y.; Yang, S.; Andersen, K.H.; Yang, Q.; Wang, Y. Thixotropy of soft clay: A review. *Eng. Geol.* **2021**, *287*, 106097. [[CrossRef](#)]
2. Cheng, W.C.; Li, G.; Liu, N.; Xu, J.; Horpibulsuk, S. Recent massive incidents for subway construction in soft alluvial deposits of Taiwan: A review. *Tunn. Undergr. Space Technol.* **2020**, *96*, 103178.1–103178.18. [[CrossRef](#)]
3. Al-Janabi, H.A.; Aubeny, C.P. Experimental measurement of thixotropy and sensitivity in gulf of Mexico clay. In Proceedings of the International Society of Offshore and Polar Engineers, Honolulu, HI, USA, 16–21 June 2019.
4. Ruge, J.C.; Molina-Gómez, F.; Rojas, J.P. Thixotropic behaviour study of clayey soils from the lacustrine deposits of Bogotá high plateau. *J. Phys. Conf. Ser.* **2019**, *1386*, 012050. [[CrossRef](#)]
5. Kamil, A.S.; Aljorany, A.N. Thixotropic hardening of fao clay. *J. Eng.* **2019**, *25*, 68–78. [[CrossRef](#)]
6. Shahriar, A.R.; Jadid, R. An experimental investigation on the effect of thixotropic aging on primary and secondary compression of reconstituted dredged clays. *Appl. Clay Sci.* **2018**, *162*, 524–533. [[CrossRef](#)]
7. Zeng, L.L.; Hong, Z.S.; Cui, Y.J. Time-dependent compression behaviour of dredged clays at high water contents in China. *Appl. Clay Sci.* **2016**, *123*, 320–328. [[CrossRef](#)]
8. Yin, Z.Y.; Karstunen, M.; Chang, C.S.; Asce, M. Modeling time-dependent behavior of soft sensitive clay. *J. Geotech. Geoenviron. Eng.* **2011**, *137*, 1103–1113. [[CrossRef](#)]
9. Tang, B.; Zhou, B.; Xie, L.; Yin, J. Evaluation method for thixotropy of clay subjected to unconfined compressive test. *Front. Earth Sci.* **2021**, *9*, 683454. [[CrossRef](#)]
10. Zhang, X.W.; Kong, L.W.; Yang, A.W.; Sayem, H.M. Thixotropic mechanism of clay: A microstructural investigation. *Soils Found.* **2017**, *57*, 23–35. [[CrossRef](#)]
11. Shahriar, A.R.; Abedin, M.Z.; Jadid, R. Thixotropic aging and its effect on 1-D compression behavior of soft reconstituted clays. *Appl. Clay Sci.* **2018**, *153*, 217–227. [[CrossRef](#)]
12. Alam, M.K.; Shahriar, A.R.; Islam, M.S.; Abedin, M.Z. Experimental investigation on the strength and deformation aspects of thixotropic aging in reconstituted clays. *Geotech. Geol. Eng.* **2021**, *39*, 2471–2486. [[CrossRef](#)]

13. Seng, S.; Tanaka, H. Properties of very soft clays: A study of thixotropic hardening and behavior under low consolidation pressure. *Soils Found.* **2012**, *52*, 335–345. [[CrossRef](#)]
14. Dexter, A.R.; Horn, R.; Kemper, W.D. Two mechanisms for age-hardening of soil. *J. Soil Sci.* **1988**, *39*, 163–175. [[CrossRef](#)]
15. Barnes, H.A. Thixotropy—a review. *J. Non-Newton. Fluid Mech.* **1997**, *70*, 1–33. [[CrossRef](#)]
16. Dullaert, K.; Mewis, J. A structural kinetics model for thixotropy. *J. Non-Newton. Fluid Mech.* **2006**, *139*, 21–30. [[CrossRef](#)]
17. Chao, Y.; Carter, J.P.; Sheng, D.; Sloan, S.W. An isotach elastoplastic constitutive model for natural soft clays. *Comput. Geotech.* **2016**, *77*, 134–155.
18. Tang, B.; Zhou, B.; Xie, L.; Yin, J.; Zhao, S.; Wang, Z. Strength recovery model of clay during thixotropy. *Adv. Civ. Eng.* **2021**, *2021*, 8825107. [[CrossRef](#)]
19. Landro, G.; Brumaud, C.; Plötze, M.L.; Winnefeld, F.; Habert, G. A fresh look at dense clay paste: Deflocculation and thixotropy mechanisms. *Colloids Surf. A Physicochem. Eng. Asp.* **2018**, *539*, 252–160. [[CrossRef](#)]
20. Du, M.; Liu, P.; Wang, J.E.; Clode, P.L.; Liu, J.; Leong, Y.K. Colloidal forces, microstructure and thixotropy of sodium montmorillonite (SWy-2) gels: Roles of electrostatic and van der Waals forces. *Appl. Clay Sci.* **2020**, *195*, 105710. [[CrossRef](#)]
21. Peng, J.; Luo, S.; Wang, D.; Ren, Y.; Zhang, G. Quantitative evaluation of thixotropy-governed microfabric evolution in soft clays. *Appl. Clay Sci.* **2021**, *210*, 106157. [[CrossRef](#)]
22. Rinaldi, V.A.; Clariá, J.J. Time dependent stress–strain behavior of bentonite slurries; effect of thixotropy. *Powder Technol.* **2016**, *291*, 311–321. [[CrossRef](#)]
23. Huo, H.F.; Qi, L.; Lei, H.Y.; Yu, G. Consideration and experimental study on thixotropy of Tianjin soft clay. *Chin. J. Rock Mech. Eng.* **2016**, *35*, 631–637.
24. Zhang, X.W.; Kong, L.W.; Li, J.; Yang, A.W. Microscopic mechanism of strength recovery in thixotropic process of clay. *Chin. J. Geotech. Eng.* **2014**, *36*, 1407–1413.
25. Shen, S.L.; Jiang, Y.Q.; Cai, F.X.; Xu, Y.S. Mechanisms of Property Changes of Soft Clays Around Deep Mixing Column. *Chin. J. Rock Mech. Eng.* **2005**, *24*, 4320–4327.
26. Tang, B.; Xie, L.; Wang, W.; Zhou, B.H.; Gong, Y.X. Unconfined compressive strength and pore structure evolution law of structural clay after disturbance. *Front. Earth Sci.* **2022**, *10*, 932621. [[CrossRef](#)]
27. Duncan, J.M.; Chang, C.Y. Nonlinear analysis of stress and strain in soils. *J. Soil Mech. Found. Div.* **1970**, *96*, 1629–1653. [[CrossRef](#)]